Acta Crystallographica Section B
Structural Science
ISSN 0108-7681

addenda and errata

Structures of the pseudo-trigonal polymorphs of $Cu_2(OH)_3Cl$. Corrigendum

Thomas Malcherek* and Jochen Schlüter

Mineralogisch-Petrographisches Institut, Universität Hamburg, Grindelallee 48, D-20146 Hamburg, Germany

Correspondence e-mail: thomas.malcherek@uni-hamburg.de

An error in the paper by Malcherek & Schlüter (2009), *Acta Cryst.* B**65**, 334–341, is corrected.

An error in the paper by Malcherek & Schlüter [*Acta Cryst.* (2009). B**65**, 334–341] is corrected. The word anatacamite is used incorrectly in Table 2 to represent the triclinic phase of $Cl_{1.015}Cu_{1.978}H_3Ni_{0.028}O_3$. This name should not have been used because it has not been approved by the IMA Commission on New Minerals, Nomenclature and Classification.

References

Malcherek, T. & Schlüter, J. (2009). *Acta Cryst.* B**65**, 334–341.

  doi:10.1107/S0108768109020916

Acta Crystallographica Section B
Structural Science
ISSN 0108-7681

Structures of the pseudo-trigonal polymorphs of $Cu_2(OH)_3Cl$

Thomas Malcherek* and Jochen Schlüter

Mineralogisch-Petrographisches Institut, Universität Hamburg, Grindelallee 48, D-20146 Hamburg, Germany

Correspondence e-mail: thomas.malcherek@uni-hamburg.de

Received 2 February 2009
Accepted 14 April 2009

The crystal structure of $Cu_2(OH)_3Cl$ has been determined using two natural samples with almost ideal stoichiometry. While one of the samples exhibits a twinned clinoatacamite structure, the other sample is characterized by the appearance of additional weak diffraction maxima at half integer positions of h and k. Structure refinement was carried out with the space group $P\bar{1}$. The relationship between the triclinic phase, clinoatacamite, paratacamite and the herbertsmithite structure is discussed in terms of symmetry as a function of Cu concentration.

1. Introduction

Pure $Cu_2(OH)_3Cl$ so far has been known to occur in the form of the three polymorphs atacamite, botallackite and clinoatacamite. While atacamite is orthorhombic the other two polymorphs are monoclinic. Another, rhombohedral structure type of $Cu_2(OH)_3Cl$ (paratacamite) has been described by Fleet (1975), but it is now believed that the rhombohedral substructure of paratacamite has to be stabilized by partial substitution of Zn or Ni for Cu (Jambor *et al.*, 1996) at ambient temperature. The Zn end member of such a solid solution, $Cu_3Zn(OH)_6Cl_2$, has been described as the mineral herbertsmithite (Braithwaite *et al.*, 2004). Recently Clissold *et al.* (2007) reported the crystal structure of gillardite, the Ni analogue of herbertsmithite. According to the experimental work of Jambor *et al.* (1996), clinoatacamite is the stable phase for compositions with up to 6% Zn per formula unit, while Zn-stabilized paratacamite occurs beyond this. According to Jambor *et al.* (1996), clinoatacamite constitutes the thermodynamically stable phase of $Cu_2(OH)_3Cl$ at ambient temperatures. While atacamite and botallackite are very resistant to Zn substitution, Zn can enter the clinoatacamite structure if large Zn concentrations are available during formation (Braithwaite *et al.*, 2004). Zn occupies the exclusively OH-coordinated Cu1 site of clinoatacamite, thereby reducing its Jahn–Teller distortion. This gives rise to the formation of Zn-stabilized paratacamite and herbertsmithite. The aim of the present work is to analyse the structural distortion of herbertsmithite or gillardite as a function of Cu uptake.

Apart from their occurrence as corrosion products of copper, the $Cu_2(OH)_3Cl$ polymorphs have recently attracted much attention for their magnetic properties (Zheng, Kawae *et al.*, 2005; Zheng, Kubozono *et al.*, 2005; Wills & Henry, 2008; Kim *et al.*, 2008). The structure of clinoatacamite has been previously determined by Grice *et al.* (1996) in space-group symmetry $P2_1/n$. The crystal structure of $Cu_2(OH)_3Cl$ is

Table 1
Electron-microprobe analysis.

Constituent	Wt %	Range	Composition†
Sample #1			
CuO	74.24 (62)	73.15–76.06	1.978 (8)
ZnO	0.02 (3)	0–0.15	0.0
NiO	0.99 (23)	0.38–1.29	0.028 (7)
Cl	16.98 (13)	16.73–17.33	1.02 (2)
H_2O‡	12.74 (13)	12.48–13.03	–
O ≡ Cl	−3.83	−3.91 to −3.77	–
Total	101.16 (60)	100.00–102.69	–
Sample #2			
CuO	71.89 (58)	70.15–72.93	1.92 (1)
ZnO	1.92 (42)	1.50–3.18	0.06 (1)
Cl	15.82 (15)	15.58–16.19	0.95 (1)
H_2O‡	12.74 (11)	12.56–12.98	–
O ≡ Cl	−3.57 (3)	−3.65 to −3.51	–
Total	98.81 (63)	97.97–100.3	–

† Based on 3(OH). ‡ Based on equimolar O and H.

described in the following using rhombohedral, monoclinic and triclinic structure models.

1.1. Group-theoretical considerations

It is assumed that the substructure of paratacamite with the space group $R\bar{3}m$, described by Fleet (1975), represents the aristotype structure of the pseudo-trigonal $Cu_2(OH)_3Cl$ polymorphs. Herbertsmithite actually exhibits this aristotype structure, stabilized by substitution of one quarter of the Cu atoms, those located at the Cu1 positions, by Zn. By gradual replacement of Zn with Cu a chain of subgroups of $R\bar{3}m$ should eventually arrive at the true symmetry of pure $Cu_2(OH)_3Cl$. In the context of the known crystal structures of $Cu_2(OH)_3Cl$ two such chains are of particular interest:

(i) $R\bar{3}m$–$R\bar{3}$–$P\bar{1}$ and

(ii) $R\bar{3}m$–$C2/m$–$P2_1/c$–$P\bar{1}$ (Ivantchev *et al.*, 2000).

The primary order parameters and their associated isotropy subgroups yielding these symmetries are conveniently explored with the aid of the *ISODISPLACE* application (Campbell *et al.*, 2006) by searching over all special *k* points of the first Brillouin Zone (BZ) in space group $R\bar{3}m$.

The crystal structure of ordered paratacamite in the space group $R\bar{3}$ is obtained from the aristotype by a transformation of index 8. The transformation matrix is $[\bar{2}00][0\bar{2}0][001]$ (by rows). The primary distortion transforms according to the F_{2+} representation of $R\bar{3}m$. The only further translationally invariant distortion permitted by group theory would be to the space group $P\bar{1}$.

Clinoatacamite has a doubled cell volume with respect to the reduced cell of the aristotype structure. The structure is obtained from the aristotype by a transformation of index 6. The transformation matrix is [1/3 2/3 −1/3][1 0 0][−2/3 −4/3 −1/3] for the space group setting $P2_1/n$ (cell choice 2). Again the active representation of $R\bar{3}m$ is F_{2+}. It is informative to look at the possible Zn uptake of paratacamite, considering Cu1 and Cu2 (which both correspond to Cu1 of the subcell; Fleet, 1975) as the preferred sites. One site accounts for 6.25% of the Cu atoms in the primitive rhombohedral cell. If the Zn content falls below this margin, some Cu inevitably has to occupy all of the Cu1 positions. It is the Jahn–Teller distortion of the regular $Cu(OH)_6$ octahedron associated with this site that drives the monoclinic distortion towards clinoatacamite. The margin of 6.25% is in good agreement with the upper stability limit of clinoatacamite found by Jambor *et al.* (1996).

Finally a triclinic distortion of the aristotype structure with appropriate cell multiplication to accomodate the additional X-ray diffraction maxima involves the primary modes F_{1+} or F_{2+}. The transformation matrix is [−4/3 −2/3 1/3][2/3 −2/3 1/3][2/3 4/3 1/3] in this case. An alternative pathway involves clinoatacamite as the stable phase at elevated temperatures and a structural phase transition to a triclinic polymorph on cooling to ambient temperature. Based on the same cell setting as obtained by the previous transformation matrix, triclinic distortion of the clinoatacamite structure with simultaneous cell doubling is associated with the D point $-\frac{1}{2}, \frac{1}{2}, 0$ of the first BZ. The distortional mode associated with the primary order parameter is then D_1D_2. The appropriate transformation from the $P2_1/n$ setting is [0 0 1][1 $\bar{1}$ 0][1 1 0]. The transition from an intermediate clinoatacamite phase is potentially continuous, as opposed to the transition from the $R\bar{3}m$ aristotype.

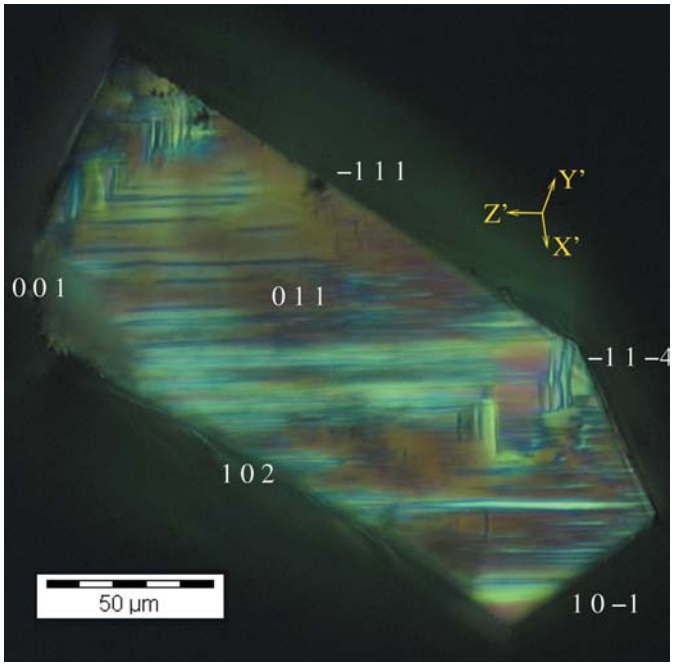

Figure 1
Optical micrograph of the measured crystal of sample #1 under crossed polarizers. Face indices refer to the hexagonal cell setting. *X*′, *Y*′, *Z*′ are the projections of the strain reference axis into the 011 plane.

2. Experimental

Two natural specimens from the Sierra Gorda district in Northern Chile have been analysed: specimen #1 originates

Table 2
Crystal data and refinement details.

Four different models have been considered in the case of sample #1. Of these only the refinements in space groups $P\bar{1}$ and $R\bar{3}$ provide a complete description of the measured data. The other two models constitute substructures of $Cu_2(OH)_3Cl$.

Sample	#1				#2
Crystal data					
Chemical formula	$Cl_{1.015}Cu_{1.978}H_3Ni_{0.028}O_3$				$Cl_{0.95}Cu_{1.92}H_3O_3Zn_{0.06}$
M_r	214.346				213.433
Name	Anatacamite	Paratacamite	Sub-paratacamite	Clinoatacamite	Clinoatacamite
Crystal system	Triclinic	Hexagonal	Hexagonal	Monoclinic	Monoclinic
Space group	$P\bar{1}$	$R\bar{3}$	$R\bar{3}m$	$P2_1/n$	$P2_1/n$
Temperature (K)	294				
a (Å)	9.1646 (9)	13.7178 (9)	6.8589 (7)	6.1675 (7)	6.1226 (3)
b (Å)	9.2029 (8)	13.7178 (9)	6.8589 (7)	6.8327 (8)	6.8346 (4)
c (Å)	9.2102 (8)	14.0639 (8)	14.0639 (15)	9.1517 (4)	9.1841 (6)
α (°)	95.858 (6)	90	90	90	90
β (°)	96.290 (7)	90	90	99.492 (2)	99.577 (4)
γ (°)	96.507 (2)	120	120	90	90
V (Å^3)	761.97 (12)	2292.0 (2)	573.0 (1)	380.38 (6)	378.96 (4)
Z	8	24	6	4	4
Radiation type	Mo $K\alpha$				Mo $K\alpha$
μ (mm^{-1})	11.693				11.604
Crystal form, size (mm)	Tabular, 0.19 × 0.12 × 0.03				Irregular, 0.08 × 0.08 × 0.05
Data collection					
Diffractometer	Nonius KappaCCD				
Data collection method	φ scans and ω scans with κ offsets				
Absorption correction	Numerical				Multi-scan
T_{min}	0.148				0.35
T_{max}	0.708				0.54
No. of measured, independent and observed reflections	47 586, 6622, 4581	47 586, 2234, , 1984	47 586, 340, , 340	47 586, 1669, , 1600	1685, 1672, 993
Criterion for observed reflections	$I>3\sigma(I)$				
R_{int}	0.045	0.105	0.062	0.045	0.0733
θ_{max} (°)	35				35.55
Refinement					
Refinement on	F^2				
$R[F^2>3\sigma(F^2)]$	0.041	0.057	0.026	0.027	0.040
$wR[F^2>3\sigma(F^2)]$	0.163	0.207	0.167	0.106	0.103
S	1.33	1.84	1.68	1.01	1.08
No. of reflections	6622	2234	340	1669	1672
No. of parameters	262	89	19	70	69
H-atom treatment	Restrained				
$(\Delta/\sigma)_{max}$	−0.0020	0.0012	−0.0021	0.0012	0.0002
$\Delta\rho_{max}$, $\Delta\rho_{min}$ e Å^{-3}	0.80, −1.49	0.84, −1.67	0.42, −0.52	0.36, −0.33	1.8, −1.93

Computer programs: *COLLECT* (Bruker AXS BV, 1997–2004), *HKL DENZO* and *SCALEPACK* (Otwinowski & Minor, 1997), *JANA*2000 (Petrícek *et al.*, 2000).

from the Vendida mine. The phase of interest occurs in tabular green crystals with {01$\bar{1}$} (clinoatacamite indexing) as the dominant form. The crystals exhibit distinctive pseudo-merohedral twinning (Fig. 1) and grow on atacamite. Specimen #2 is from the Santa Catalina mine. Here clinoatacamite occurs together with brochantite, herbertsmithite and atacamite.

Analyses (Table 1) were obtained using a Cameca SX 100 microprobe operating in wavelength dispersion mode with an accelerating voltage of 15 kV, a specimen current of 20 nA and focused beam. Vanadinite, CuO, ZnS and NiO were used as standards for Cl, Cu, Zn and Ni, respectively. Sample #1 also showed traces of Mn and Cd. 50 points and 20 points were measured for samples #1 and #2, respectively. The crystal of sample #2 used for the microprobe analysis is a fragment of the crystal studied by X-ray diffraction.

Suitable crystal fragments of both specimens have been selected for X-ray single-crystal diffraction. Diffraction data were collected using a Nonius KappaCCD diffractometer with Mo $K\alpha$ radiation (Table 2[1]). The data have been integrated using *DENZO SMN* (Otwinowski & Minor, 1997) and processed using *WinGX* (Farrugia, 1999). An empirical absorption correction has been applied to the data from sample #2 using *SORTAV* (Blessing, 1995), as implemented in *WinGX*. Owing to the larger size and to the presence of some well developed faces for specimen #1, diffraction data have been treated with a Gaussian absorption correction in this case. Undistorted representations of reciprocal space have been calculated using software developed in-house. Intensity integration for sample #1 has been performed on the basis of a triclinic, pseudo-rhombohedral primitive lattice. Post-refine-

[1] Supplementary data for this paper are available from the IUCr electronic archives (Reference: HW5003). Services for accessing these data are described at the back of the journal.

Table 3
Lattice parameters of clinoatacamite transformed to a pseudo-hexagonal setting (*a*) and calculated spontaneous strain tensor elements with corresponding scalar strain (*b*).

(*a*) Sample	$X_{Zn,Ni}$†	a_R	b_R	c_R	α_R	β_R	γ_R
#1	0.014	6.8391	6.8327	14.0952	90.0	89.515	119.969
#1 (triclinic)	0.014	6.8431	6.8342	14.0925	90.132	89.482	119.871
#2	0.030	6.8421	6.8346	14.0310	90.0	90.006	119.964
Oswald & Guenter (1971)‡	0	6.8298	6.8200	14.0640	90.0	89.291	119.953
Zheng, Kawae *et al.* (2005)	0	6.8257	6.8166	14.0484	90.0	89.302	119.956
Grice *et al.* (1996	0	6.8129	6.8050	14.0311	90.0	89.473	119.962

(*b*) Sample	e_{11}	e_{22}	e_{33}	e_{12}	e_{13}	e_{23}	$(\sum e_{ij}^2)$
#1	0.0011	−0.0002	0.0014	0.0	0.0049	0.0	0.0071
#1 (triclinic)	0.0026	0.0	0.0012	0.0008	0.0046	−0.0012	0.0073
#2	0.0015	0.0001	−0.0031	0.0	0.0	0.0	0.0035
Oswald & Guenter (1971)	−0.0003	−0.0020	−0.0009	0.0	0.007	0.0	0.0103
Zheng, Kawae *et al.* (2005)	−0.0008	−0.0025	−0.0020	0.0	0.007	0.0	0.0105
Grice *et al.* (1996)	−0.0027	−0.0042	−0.0032	0.0	0.005	0.0	0.0096

† $X_{Zn,Ni} = (X_{Zn} + X_{Ni})/(X_{Cu} + X_{Zn} + X_{Ni})$. ‡ Transformed from $P2_1/a$ setting.

ment has been carried out with this and with a C-centred monoclinic lattice ($a' = 2a$, $b' = 2b$ with respect to clinoatacamite in Table 2). The diffraction intensities of sample #2 have been integrated using cell parameters with a doubled *c*-repeat relative to clinoatacamite. Transformation to the clinoatacamite cell yielded the data used for structure refinement. Owing to the similar scattering power of Cu, Zn and Ni, cation sites have been assumed to be fully occupied by Cu in all refinements. Nearest-neighbour O—H bonds have been restrained to a length of 1.0 Å.

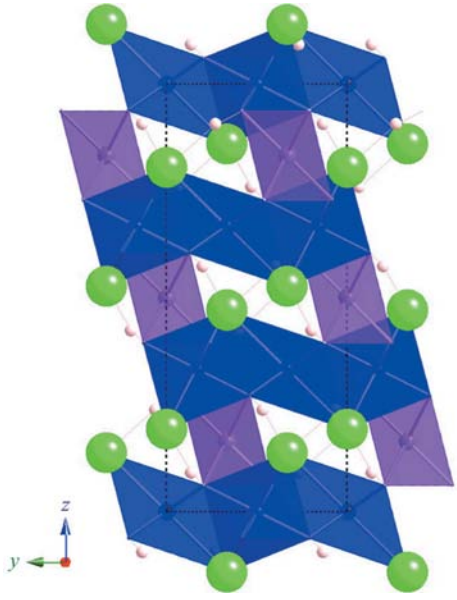

Figure 2
The $R\bar{3}m$ paratacamite substructure in a polyhedral representation. Green spheres represent Cl, small pink spheres represent H. Interlayer Cu polyhedra are colored in magenta, intralayer polyhedra in blue.

3. Results and discussion

The aristotype of the pseudo-trigonal $Cu_2(OH)_3Cl$ polymorphs (Fig. 2) forms a network of edge-sharing distorted octahedra. Within layers normal to the trigonal axis Cu atoms are axially coordinated by two Cl and equatorially coordinated by four OH (intra-layer octahedra). The layers are connected by $Cu(OH)_6$ octahedra (inter-layer octahedra) that share edges with the intra-layer octahedra. Jahn–Teller distortion of the inter-layer octahedra drives the transition to the lower symmetry polymorphs. In order to analyse the lattice distortion involved, it is helpful to transform the monoclinic clinoatacamite cell to a hexagonal cell setting. This transformation is achieved by application of the matrix [1/2 1/2 −1/2][0 $\bar{1}$ 0][2 0 1] (by rows). Thus, [201] of the monoclinic lattice becomes the threefold inversion axis of the aristotype.

Table 3 lists the transformed lattice parameters along with the derived components of the strain tensor. The components have been calculated according to the following equations

$$e_{11} = \frac{2a\sin\gamma}{a_0(3)^{1/2}} - 1 \quad (1)$$

$$e_{22} = \frac{b}{a_0} - 1 \quad (2)$$

$$e_{33} = \frac{c\sin\alpha\sin\beta^*}{c_0} - 1 \quad (3)$$

$$e_{23} = \frac{c\cos\alpha}{2c_0} \quad (4)$$

$$e_{13} = -\frac{c\sin\alpha\cos\beta^*}{2c_0} \quad (5)$$

$$e_{12} = \frac{1}{a_0(3)^{1/2}}\left(a\cos\gamma + \frac{b}{2}\right), \quad (6)$$

which have been derived from the general equations given by Carpenter *et al.* (1998) with $\alpha_0 = \beta_0 = 90$, $\gamma_0 = 120^\circ$ and $b_0 = a_0$. The lattice parameters of herbertsmithite (Braithwaite *et al.*, 2004) can act as suitable reference values. Thus, $a_0 = 6.834$ and $c_0 = 14.075$ Å. Strictly speaking this reference state is a valid approximation only for Zn substitution, as the end-member volume of $Cu_3Ni(OH)_6Cl_2$ is considerably smaller (c = 13.8459 Å; *cf.* Clissold *et al.*, 2007), owing to the smaller cation radius of Ni compared with Zn. However, for the small Ni concentration found in sample #1, the additional volume strain is expected to be negligible.

The scalar strain given in the final column of Table 3(*b*) demonstrates that the distortion of the rhombohedral cell is generally very small and that it systematically decreases with increasing impurity content (Fig. 3). Allowing for triclinic distortion of sample #1 yields scalar strain very similar to the monoclinic setting.

Table 4
Refined atomic positions and thermal displacement parameters (Å^2) of clinoatacamite for the substructure of sample #1 (first line) and for sample #2 (second line).

Position	BVS	x	y	z	U^{11}	U^{22}	U^{33}	U^{12}	U^{13}	U^{23}
Cu1	1.95	0	1/2	1/2	0.0119 (2)	0.0131 (2)	0.0091 (2)	−0.0014 (1)	0.0005 (1)	0.0004 (1)
	1.91	0	1/2	1/2	0.0130 (3)	0.0139 (3)	0.0129 (3)	−0.0006 (2)	0.0033 (2)	−0.0004 (3)
Cu2	2.01	0	0	0	0.0127 (2)	0.0113 (2)	0.0125 (2)	0.0010 (1)	0.0051 (2)	0.0000 (1)
	2.02	0	0	0	0.0161 (3)	0.0164 (3)	0.0156 (3)	−0.0001 (3)	0.0067 (2)	−0.0003 (3)
Cu3	1.98	0.25920 (5)	0.23666 (7)	0.74865 (2)	0.0153 (2)	0.0114 (2)	0.0097 (2)	0.0018 (1)	0.0029 (1)	0.0017 (1)
	2.01	0.25292 (8)	0.24557 (5)	0.74944 (6)	0.0181 (2)	0.0127 (2)	0.0156 (2)	0.0008 (1)	0.0057 (2)	0.0013 (1)
Cl	1.01	0.1117 (1)	0.99576 (6)	0.30678 (8)	0.0164 (3)	0.0168 (3)	0.0148 (3)	−0.0007 (1)	0.0008 (2)	0.0009 (1)
	1.06	0.1124 (2)	0.9986 (1)	0.3061 (1)	0.0181 (4)	0.0187 (4)	0.0173 (4)	0.0002 (4)	0.0039 (3)	0.0008 (4)
O1	1.96	0.3068 (3)	0.2917 (3)	0.5480 (2)	0.0253 (8)	0.0138 (7)	0.0110 (6)	−0.0061 (5)	0.0054 (5)	−0.0017 (5)
	1.89	0.2809 (6)	0.3056 (4)	0.5432 (3)	0.035 (2)	0.021 (1)	0.019 (1)	−0.013 (1)	0.011 (1)	−0.007 (1)
O2	1.99	0.4221 (4)	0.9822 (2)	0.7757 (3)	0.0139 (7)	0.0123 (6)	0.0125 (7)	0.0001 (5)	0.0043 (6)	−0.0005 (4)
	1.88	0.415658	0.9945 (4)	0.7679 (4)	0.017 (1)	0.015 (1)	0.040 (2)	0.002 (1)	0.015 (1)	−0.002 (1)
O3	2.06	0.2577 (3)	0.6798 (3)	0.5400 (2)	0.0160 (6)	0.0135 (7)	0.0109 (5)	0.0005 (5)	0.0026 (5)	0.0024 (5)
	1.95	0.2675 (5)	0.6845 (4)	0.5410 (3)	0.029 (2)	0.016 (1)	0.019 (1)	0.006 (1)	0.010 (1)	0.005 (1)
H1	1.03	0.281 (7)	0.181 (5)	0.486 (4)	0.026 (7)	–	–	–	–	–
	0.93	0.22 (2)	0.20 (1)	0.47 (1)	0.16 (3)	–	–	–	–	–
†	–	0.2385	0.208	0.4726	–	–	–	–	–	–
H2	1.02	0.552 (7)	0.982 (4)	0.727 (6)	0.026	–	–	–	–	–
	0.95	0.580 (5)	0.993 (8)	0.78 (2)	0.16	–	–	–	–	–
†	–	0.5527	0.022	0.7307	–	–	–	–	–	–
H3	1.02	0.246 (7)	0.795 (5)	0.477 (4)	0.026	–	–	–	–	–
	0.93	0.23 (3)	0.79 (1)	0.47 (1)	0.16	–	–	–	–	–
†	–	0.2798	0.8146	0.4787	–	–	–	–	–	–

† Transformed deuterium positions of Wills & Henry (2008).

Initial refinement of sample #1 has been conducted starting with the parameters for ordered paratacamite (Fleet, 1975). Apart from the small but significant metric distortion from rhombohedral symmetry, a high value of $R_{\rm int}$ and a relatively large residual of 0.057 suggest that the true symmetry is lower than $R\bar{3}$. Note that the residual of the paratacamite refinement is not much higher than the value of 0.051 originally given by Fleet (1975). Possible obverse–reverse twinning has been considered in the present refinement. Lower than rhombohedral symmetry is also indicated by the obvious twinning observed in the optical micrograph (Fig. 1). Domain boundaries occur parallel to the projection of the pseudo-trigonal axis (Z' in Fig. 1) and normal to it.

Refinement with the clinoatacamite structure yields low residuals and a plausible crystal structure, but it only accounts for half of the nominally observed reflections (Fig. 4). The restrained hydrogen positions of the clinoatacamite model

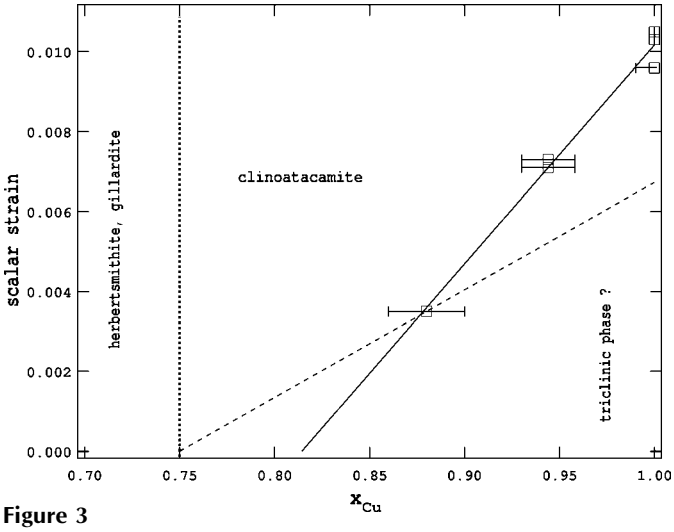

Figure 3
Scalar strain as a function of Cu concentration in $Cu_3Cu_x(Zn,Ni)_{1-x}(OH)_6Cl_2$. The vertical line marks the theoretical boundary between herbertsmithite and clinoatacamite. The dashed line extrapolates the expected scalar strain of clinoatacamite.

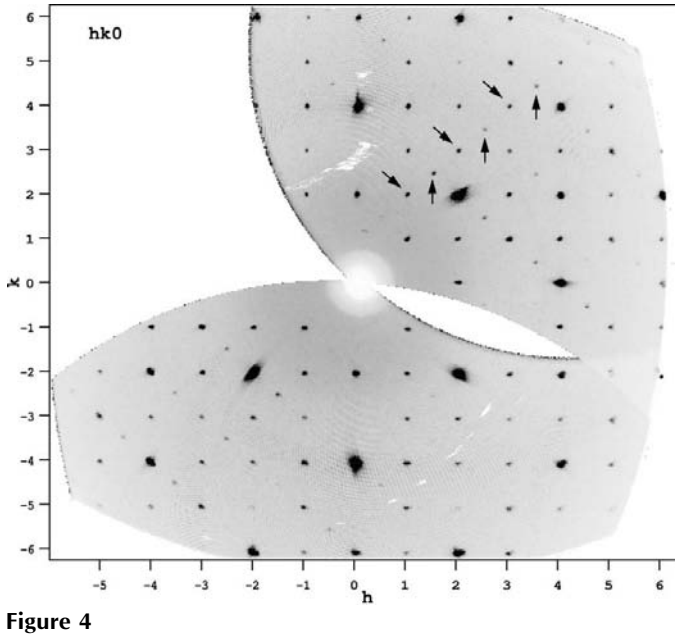

Figure 4
Top: Reconstructed layer of the reciprocal lattice for sample #1, showing additional maxima at half-integer positions of h and k (*e.g.* upwards arrows, indices are relative to clinoatacamite). The additional maxima represent the D point of the clinoatacamite BZ. Diagonal arrows indicate selected reflections characteristic of clinoatacamite, *i.e.* representing the F-point of the aristotype BZ.

Table 5
Comparison of bond-valence sums for the triclinic model ($P\bar{1}$) and for ordered paratacamite ($R\bar{3}$).

Position	$P\bar{1}$	$R\bar{3}$	Position	$P\bar{1}$	$R\bar{3}$
Cu1*a*	1.90	1.94	O2*c*	1.96	1.86
Cu2*a*	1.92	1.82	O3*a*	1.99	1.99
Cu2*b*	1.97	1.82	O3*b*	2.04	1.99
Cu2*c*	1.95	1.82	O3*c*	2.11	1.99
Cu3*a*	1.93	1.96	O4*a*	1.88	1.97
Cu3*b*	2.01	1.96	O4*b*	2.05	1.97
Cu3*c*	2.03	1.96	O4*c*	2.01	1.97
Cu4*a*	2.00	2.02	H1*a*	0.94	1.02
Cu4*b*	1.92	2.02	H1*b*	0.96	1.02
Cu4*c*	2.02	2.02	H1*c*	0.95	1.02
Cl1*a*	1.07	1.19	H2*a*	1.00	0.99
Cl2*a*	0.94	0.96	H2*b*	0.97	0.99
Cl2*b*	1.03	0.96	H2*c*	1.00	0.99
Cl2*c*	1.03	0.96	H3*a*	1.03	1.05
O1*a*	1.89	2.04	H3*b*	0.99	1.05
O1*b*	1.91	2.04	H3*c*	1.07	1.05
O1*c*	1.95	2.04	H4*a*	0.99	0.94
O2*a*	1.92	1.86	H4*b*	1.00	0.94
O2*b*	1.92	1.86	H4*c*	1.04	0.94

agree well with appropriately transformed deuterium positions obtained by neutron diffraction measurements (Wills & Henry, 2008; *cf.* Table 4). Three twin domains contribute to the clinoatacamite diffraction signal with volume fractions of 73, 12 and 15%. The corresponding operations are a 120° turn about [201] and a mirror plane normal to $[11\bar{1}]$.

The paratacamite substructure also yields low residuals, but it again halves the number of reflections accounted for by the clinoatacamite structure. Reflections with $h + k + l$ = odd in the $P2_1/n$ clinoatacamite setting transform to half integer indices h or k in the hexagonal setting. This latter condition corresponds to the critical F-point of the BZ associated with $R\bar{3}m$.

The initially obtained ordered paratacamite structure was finally transformed to space group $P\bar{1}$ in a pseudo-rhombohedral lattice setting. Parameter refinement slowly converged to a residual of 0.041. Starting values for the hydrogen positions were obtained from the paratacamite substructure, transformed to the rhombohedral setting and subjected to soft distance restraints with respect to neighbouring O and Cl atoms (1.0 ± 0.03 and 2.2 ± 0.05 Å). Three domains contribute to the calculated intensities, with volume fractions of 43, 39 and 18%. The corresponding lost symmetry elements of $R\bar{3}m$ are the diads parallel to $[01\bar{1}]_{\rm tricl.}$ and to $[10\bar{1}]_{\rm tricl.}$. The former twin law is expected for a monoclinic to triclinic transition.

Attempts to increase the symmetry of this structure to the space group $C2/m$ by the transformation $[\bar{1}\bar{1}0][\bar{1}10][00\bar{1}]$ and subsequent origin shift of 1/4,1/4,0 yielded residuals of ~ 0.05 and unrealistically large anisotropic displacement factors at the transformed O1*b* and O2*c* positions. This was taken as an indication that the true symmetry is in fact lower than $C2/m$.

For the triclinic structure model the bond-valence sums on the basis of appropriate parameters for Cl—H and O—H bonds (Malcherek & Schlüter, 2007) agree with the formal valence of the atoms (Table 5). Good agreement is also obtained for the clinoatacamite substructure (Table 4). For the ordered paratacamite structure the Cl1 atom appears slightly overbonded, while Cu2 results underbonded (Table 5). For the paratacamite substructure no significant deviation from the formal valence is observed at the undistorted Cu1 position.

Fig. 5 shows the atomic displacements relative to the $R\bar{3}m$ aristotype structure. The coordinates refer to the pseudo-rhombohedral coordinate system of the triclinic phase. Figs. 5(*a*) and (*b*) demonstrate that the displacements associated with the clinoatacamite (sub)structure and with the ordered paratacamite structure generally agree with those obtained from previous structure refinements (Grice *et al.*, 1996; Fleet, 1975). Fig. 5(*c*) shows that the displacements associated with the triclinic crystal structure amount to subtle variations of the clinoatacamite structure. Among the Cu atoms these additional displacements, determined by the difference between the triclinic and monoclinic distortion amplitudes, are most obvious for the z coordinate of Cu3*c* and Cu4*a*. Both atoms have zero amplitude in terms of monoclinic distortion. The largest triclinic distortions are observed for the O atoms, while Cl atoms remain largely unaffected. The small size of the additional displacements and the small O-atom scattering power cause the weakness of diffraction maxima associated with the zone-boundary position that defines the triclinic supercell. Conversely, because of the inherent weakness of these superstructure reflections, large parameter correlations limit the accuracy of the obtained O-atom displacements.

Symmetry mode decomposition (Amplimodes, Aroyo *et al.*, 2006) of the triclinic structure clearly shows that F_{2+}, with an amplitude of 0.808 Å, is the primary distortion relative to the paratacamite substructure. However, more significant for the triclinic distortion is the amplitude associated with the F_{1+} mode, which amounts to 0.064 Å or 8% of the distortion associated with F_{2+} (Fig. 5).

The main effect of the triclinic distortion is a stronger puckering and shearing of the kagomè lattice of Cu atoms that is formed by the intralayer octahedra (Fig. 6). The distortion of the layers systematically increases from herbertsmithite or sub-paratacamite, where the kagomè layers are ideal, to clinoatacamite to the triclinic phase of sample #1.

Sample #2 with its lower Cu content (Table 2) refined with the clinoatacamite structure (Table 4). The seemingly doubled c-lattice repeat is caused by twinning that involves a half turn about the c^* axis (twin index 2). The twin lattice is also compatible with a C-centred orthorhombic cell with approximate parameters a = 6.11, b = 36.23 and c = 6.83 Å. This kind of twinning by reticular merohedry can be expected for monoclinic lattice parameters with $\cos\beta^* \simeq a/(4c)$. Apart from the twin reflections no additional diffraction maxima have been observed for sample #2.

It should be pointed out that paratacamite, as it was originally described by Fleet (1975), is in fact a superstructure of the herbertsmithite crystal structure. The additional diffraction maxima are weak and therefore easily overlooked. Thus, the designation of intermediate compositions $Cu_3(Cu,Zn)(OH)_6Cl_2$ as paratacamite (*i.e.* Zn-stabilized paratacamite), as has been suggested by Grice *et al.* (1996), is

problematic unless the occurrence of the $R\bar{3}$ superstructure can be verified at these compositions. It is likely that the presence of significant Zn or Ni restricts the size of ordered domains with the result that the characteristic superstructure reflections cannot be observed in this case. Braithwaite *et al.* (2004) claim that superlattice reflections have been observed for all of the (Zn-stabilized) paratacamite samples studied, however, they fail to present evidence of these reflections. The same authors suggest that the superlattice reflections arise from ordering of the Zn substitution, while the original structure refinement of ordered paratacamite was based only on atom displacements assuming pure $Cu_2(OH)_3Cl$ (Fleet, 1975). Also in our study the additional weak reflections have been reproduced without introduction of cation ordering.

In combination with the group-theoretical arguments developed above, the most likely sequence of space-group symmetries for $Cu_3Cu_x(Zn,Ni)_{1-x}(OH)_6Cl_2$ with increasing x is $R\bar{3}m$–$P2_1/n$ ($P2_1/c$)–$P\bar{1}$. Herbertsmithite (or gillardite, depending on Ni content) is thus the stable phase for $x < 0.75$. For $x \geq 0.75$ clinoatacamite is the stable phase up to at least $x = 0.88$ (Fig. 3). Linear extrapolation of the scalar strain to zero yields a limit of $x \simeq 0.82$ for the stability of clinoatacamite, above the expected value of $x = 0.75$. Conversely, extrapolation from this expected value, as shown by the dashed line in Fig. 3, results in a smaller strain for the end-member composition. However, more data are needed to verify the onset of clinoatacamite formation. For stoichiometric $Cu_2(OH)_3Cl$ clinoatacamite might also be the stable phase at elevated temperatures. The observed microstructure of sample #1 could be the result of a phase transition from clinoatacamite to the triclinic phase *via* cooling. While the potentially triclinic polymorph is easily identified by single-crystal X-ray diffraction, it will be very difficult to distinguish it from clinoatacamite in X-ray powder diffraction experiments. Calculation of the powder diffraction pattern shows that the characteristic superstructure reflections at the D point of the monoclinic BZ are too weak to be observable in any realistic experimental setting. On the other hand, deviation from the monoclinic metric is too small to induce peak splitting or significant peak broadening. Powder neutron diffraction can be expected to yield a significant intensity of the superlattice reflections, owing to the significant scattering cross section of the O atoms. It is noteworthy that published low-temperature neutron powder diffraction measurements of clinoatacamite (Wills & Henry, 2008; Kim *et al.*, 2008) do show Bragg peaks at scattering angles that coincide with

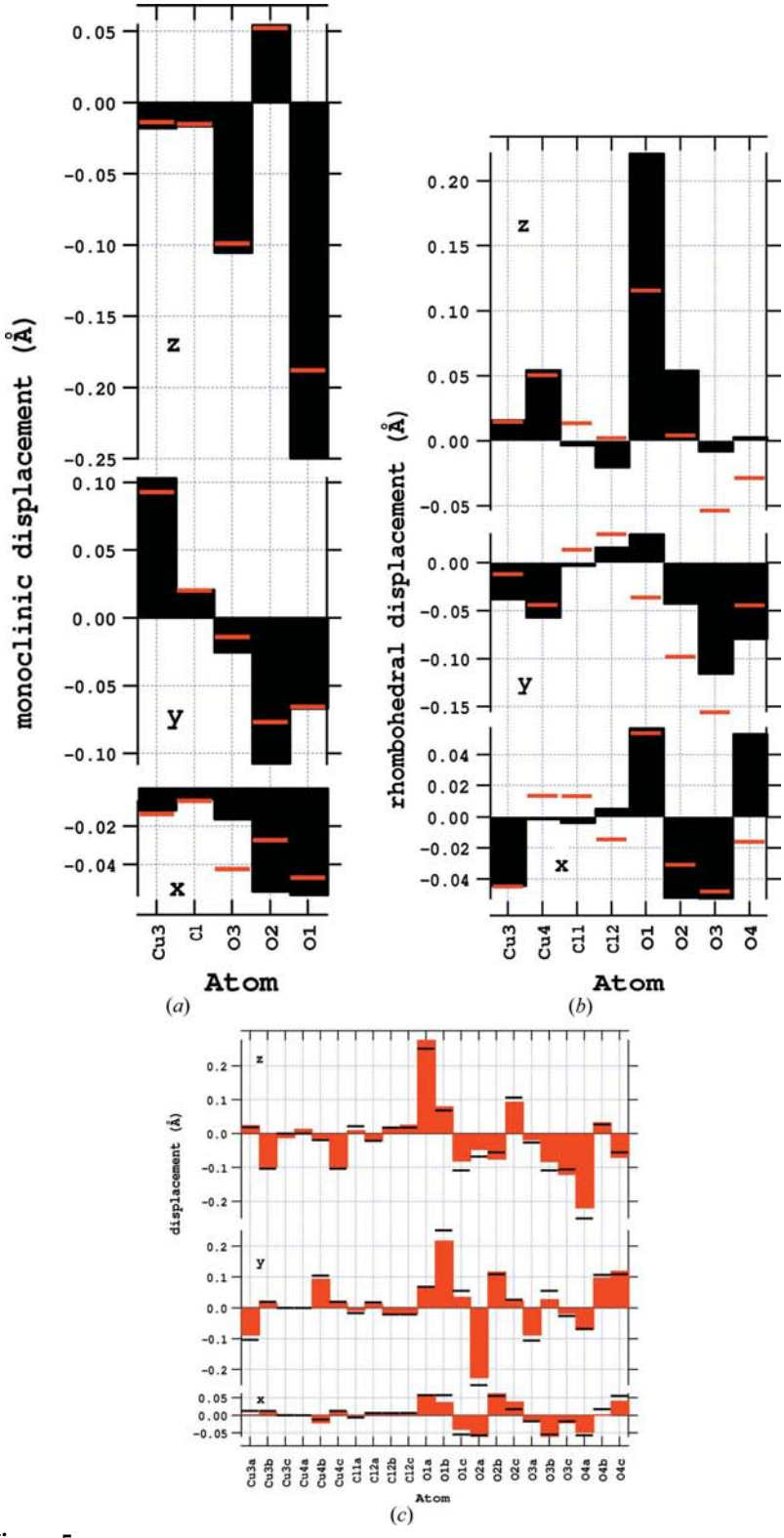

Figure 5
Atomic displacements of sample #1 with respect to the paratacamite substructure: (*a*) clinoatacamite substructure, this study (bars) and Grice *et al.* (1996) (red markers); (*b*) ordered paratacamite, this study (bars) and Fleet (1975) (red markers); (*c*) triclinic structure (red bars) and corresponding clinoatacamite displacements (black markers).

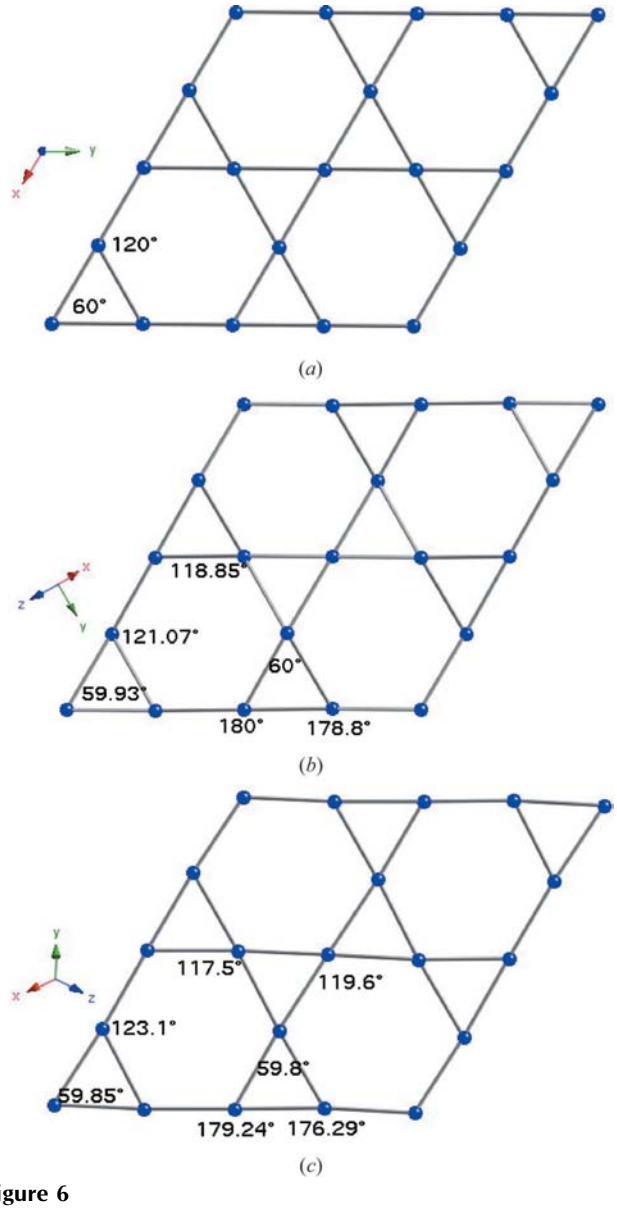

Figure 6
Selected angles of the kagomè networks formed by the intralayer Cu atoms in (*a*) herbertsmithite, (*b*) in clinoatacamite (sample #2) and (*c*) in the triclinic sample #1.

those of the expected superstructure diffraction maxima of the triclinic phase reported here.

In summary we have determined a triclinic phase of $Cu_2(OH)_3Cl$ with a high degree of trigonal and monoclinic pseudo-symmetry. Microstructure, group–subgroup relations, unit-cell size, bond-valence considerations and refinement quality favour the triclinic model over alternative stucture models of higher symmetry. The confirmation of the clinoatacamite structure for a second sample with approximately doubled impurity content suggests that clinoatacamite is stable at higher impurity concentrations than the triclinic polymorph.

The authors would like to thank S. Heidrich for conducting the electron microprobe analysis.

References

Aroyo, M. I., Perez-Mato, J. M., Capillas, C., Kroumova, E., Ivantchev, S., Madariaga, G., Kirov, A. & Wondratschek, H. (2006). *Z. Kristallogr.* **221**, 15–27.
Blessing, R. H. (1995). *Acta Cryst.* A**51**, 33–38.
Braithwaite, R. S. W., Mereiter, K., Paar, W. H. & Clark, A. M. (2004). *Mineral. Mag.* **68**, 527–539.
Bruker (1997–2004). *COLLECT*. Bruker AXS BV, Delft, The Netherlands.
Campbell, B. J., Stokes, H. T., Tanner, D. E. & Hatch, D. M. (2006). *J. Appl. Cryst.* **39**, 607–614.
Carpenter, M. A., Salje, E. K. H. & Graeme-Barber, A. (1998). *Eur. J. Miner.* **10**, 621–691.
Clissold, M. E., Leverett, P., Williams, P. A., Hibbs, D. E. & Nickel, E. H. (2007). *Can. Mineral.* **45**, 317–320.
Farrugia, L. J. (1999). *J. Appl. Cryst.* **32**, 837–838.
Fleet, M. E. (1975). *Acta Cryst.* B**31**, 183–187.
Grice, J. D., Szymańnski, J. T. & Jambor, J. L. (1996). *Can. Mineral.* **34**, 73–78.
Ivantchev, S., Kroumova, E., Madariaga, G., Pérez-Mato, J. M. & Aroyo, M. I. (2000). *J. Appl. Cryst.* **33**, 1190–1191.
Jambor, J. L., Dutrizac, J. E., Roberts, A. C., Grice, J. D. & Szymànski, J. T. (1996). *Can. Mineral.* **34**, 61–72.
Kim, J., Ji, S., Lee, S., Lake, B., Yildirim, T., Nojiri, H., Kikuchi, H., Habicht, K., Qiu, Y. & Kiefer, K. (2008). *Phys. Rev. Lett.* **101**, 107201.
Malcherek, T. & Schlüter, J. (2007). *Acta Cryst.* B**63**, 157–160.
Oswald, H. R. & Guenter, J. R. (1971). *J. Appl. Cryst.* **4**, 530–531.
Otwinowski, Z. & Minor, W. (1997). *Methods in Enzymology*, Vol. 276, pp. 307–326. New York: Academic Press.
Petrícek, V., Dusek, M. & Palatinus, L. (2000). *JANA*2000. Institute of Physics, Prague, Czech Republic.
Wills, A. S. & Henry, J. (2008). *J. Phys. Condens. Matter*, **20**, 472206.
Zheng, X. G., Kawae, T., Kashitani, Y., Li, C. S., Tateiwa, N., Takeda, K., Yamada, H., Xu, C. N. & Ren, Y. (2005). *Phys. Rev. B*, **71**, 052409.
Zheng, X. G., Kubozono, H., Nishiyama, K., Higemoto, W., Kawae, T., Koda, A. & Xu, C. N. (2005). *Phys. Rev. Lett.* **95**, 057201.